





Article

Topological Features of the Alluaudite-Type Framework and Its Derivatives: Synthesis and Crystal Structure of $\text{NaMnNi}_2(\text{H}_{2/3}\text{PO}_4)_3$

Sergey M. Aksenov ^{1,*}, Natalia A. Yamnova ², Natalia A. Kabanova ^{1,3}, Anatoly S. Volkov ^{2,4}, Olga A. Gurbanova ², Dina V. Deyneko ⁵, Olga V. Dimitrova ² and Sergey V. Krivovichev ^{6,7}

- ¹ Laboratory of Nature-Inspired Technologies and Environmental Safety of the Arctic, Kola Science Centre, Russian Academy of Sciences, 14 Fersman Str., 184209 Apatity, Russia; weterster@gmail.com
 - ² Department of Geology, Moscow State University, Vorobiev Gory, 119991 Moscow, Russia; natalia-yamnova@yandex.ru (N.A.Y.); toljha@yandex.ru (A.S.V.); gur_o@mail.ru (O.A.G.); dimitrova@list.ru (O.V.D.)
 - ³ Samara Center for Theoretical Materials Science, Samara State Technical University, Molodogvardeyskaya Str. 244, 443100 Samara, Russia
 - ⁴ Institute of Experimental Mineralogy, Russian Academy of Sciences, 4 Akademika Osip'yana Str., 142432 Chernogolovka, Russia
 - ⁵ Department of Chemistry, Moscow State University, Vorobiev Gory, 119991 Moscow, Russia; deynkomsu@gmail.com
 - ⁶ Nanomaterials Research Centre, Kola Science Center, Russian Academy of Sciences, Fersmana Str. 14, 184209 Apatity, Russia; skrivovi@mail.ru
 - ⁷ Department of Crystallography, Institute of Earth Sciences, St Petersburg State University, University Embankment 7/9, 199034 St Petersburg, Russia
- * Correspondence: aks.crys@gmail.com



Citation: Aksenov, S.M.; Yamnova, N.A.; Kabanova, N.A.; Volkov, A.S.; Gurbanova, O.A.; Deyneko, D.V.; Dimitrova, O.V.; Krivovichev, S.V. Topological Features of the Alluaudite-Type Framework and its Derivatives: Synthesis and Crystal Structure of $\text{NaMnNi}_2(\text{H}_{2/3}\text{PO}_4)_3$. *Crystals* **2021**, *11*, 237. <https://doi.org/10.3390/cryst11030237>

Received: 8 November 2020
Accepted: 24 February 2021
Published: 26 February 2021

Publisher's Note: MDPI stays neutral with regard to jurisdictional claims in published maps and institutional affiliations.



Copyright: © 2021 by the authors. Licensee MDPI, Basel, Switzerland. This article is an open access article distributed under the terms and conditions of the Creative Commons Attribution (CC BY) license (<https://creativecommons.org/licenses/by/4.0/>).

Abstract: A new sodium manganese-nickel phosphate of alluaudite supergroup with the general formula $\text{NaMnNi}_2(\text{H}_{2/3}\text{PO}_4)_3$ was synthesized by a hydrothermal method. The synthesis was carried out in the temperature range from 540 to 660 K and at the general pressure of 80 atm from the oxides mixture in the molar ratio $\text{MnCl}_2: 2\text{NiCl}_2: 2\text{Na}_3\text{PO}_4: \text{H}_3\text{BO}_3: 10\text{H}_2\text{O}$. The crystal structure was studied by a single-crystal X-ray diffraction analysis: space group $C2/c$ (No. 15), $a = 16.8913(4)$, $b = 5.6406(1)$, $c = 8.3591(3)$ Å, $\beta = 93.919(3)$, $V = 794.57(4)$ Å³. The compound belongs to the alluaudite structure type based upon a mixed hetero-polyhedral framework formed by MX_6 -octahedra and TX_4 -tetrahedra. The characteristic feature of the title compound is the absence of cations or H_2O molecules in channel II, while the negative charge of the framework is balanced by the partial protonation of PO_4 tetrahedra. The presence of the transition metals at the *A*-type sites results in the changes of stoichiometry and the local topological features. Topological analysis of the hetero-polyhedral alluaudite-type frameworks and its derivatives (johillerite-, $\text{KCd}_4(\text{VO}_4)_3$ -, and keyite-type) and quantitative characterization of their differences was performed by means of natural tilings.

Keywords: alluaudite supergroup; phosphates; topology; crystal structure; stoichiometry; transition metals; crystal chemistry; hetero-polyhedral frameworks

1. Introduction

Inorganic nickel phosphates attract interest because of their magnetic [1–4] and electrical [5–7] properties. Among them, compounds containing heteropolyhedral frameworks based upon the condensation of PO_4 tetrahedra and NiO_6 octahedra are related to zeolites and zeolite-type materials [8–11] and, owing to the presence of wide channels and cavities, possess interesting sorption and ion-exchange properties [12–15].

The alluaudite structure type (named after the mineral alluaudite, $\text{NaMnFe}^{3+}_2(\text{PO}_4)_3$ [16]) corresponds to natural oxysalts of the alluaudite supergroup [17] and synthetic compounds [18,19] with the general formula $[\text{A}2\text{A}2'\text{A}2''_2][\text{A}1\text{A}1'\text{A}1''_2]$

$\{M1M2_2(TO_4)_3\}$, where M and T are octahedral and tetrahedral cations $A1$, $A1'$, and $A1''$ are cation sites located in the channel I $A2$, $A2'$, and $A2''$ are cation sites in channel II. Figure and square brackets denote the compositions of the framework and extra framework cations, respectively [19–21]. Because of the wide isomorphism in the cationic and anionic parts of the alluaudite-type structures, they attract interest as advanced materials for Li-ion batteries [22–28]. Despite the observed chemical diversity, Ni-containing alluaudite-type compounds are represented only by anhydrous phosphates $Na_2MNi_2(PO_4)_3$ ($M = Fe, Al$) [29,30] and $CaFeNi_2(PO_4)_3$ [31], mixed phosphate-hydrogen phosphate $AgNi_3(PO_4)(HPO_4)_2$ [32], sulfate $Na_2Ni_2(SO_4)_3$ [33,34], and mixed sulfate-selenate $Na_3Ni_{1.5}(SO_4)_{3-1.5x}(SeO_4)_{1.5x}$ [35].

The present work continues our systematic study of topologic features of compounds with hetero-polyhedral frameworks [36–40] and their comparison with zeolites. Here we report the results of hydrothermal synthesis of novel mixed nickel-manganese phosphate with an alluaudite-type structure and its characterization by the means of single-crystal X-ray diffraction analysis.

2. Materials and Methods

2.1. Synthesis and Sample Characterization

Single crystals of $NaMnNi_2(H_{2/3}PO_4)_3$ (**1**) were synthesized by a hydrothermal method. The synthesis was carried out in the temperature range from 540 to 660 K and at the general pressure of 80 atm from the mixture of oxides taken in the molar ratio $MnCl_2: 2NiCl_2: 2Na_3PO_4: H_3BO_3: 10H_2O$. A standard Cu-lined stainless steel autoclave of 5 mL capacity was used. The coefficient of the autoclave filling was selected so that the pressure was constant. The experimental duration was 20 days and corresponds to the full completion of the chemical reaction. Final cooling after the synthesis experiment to room temperature was done over 24 h. The precipitate was separated by filtration and washed several times with hot distilled water and finally dried at room temperature for 12 h. The reaction products were small green crystals of the new phase in the estimated yield of 5%, which have been selected manually for the further studies.

The elemental contents of the selected crystals were determined by a Jeol JSM6480LV scanning electron microscope equipped with an INCA Wave 500 wave length spectrometer. The conditions of analysis were: accelerating voltage of 20 kV, a current of 20 nA, and a beam diameter 3 of μm . Chemical composition of **1** is (at.%): Na 5.86, Mn 6.59, Ni 9.58, P 16.56, O 61.41.

2.2. Single Crystal X-ray Diffraction Analysis

A yellow, round-shaped grain of **1** ($0.04 \times 0.05 \times 0.11 \text{ mm}^3$) was selected carefully under a polarizing microscope and used for single-crystal X-ray diffraction data collection. The single-crystal X-ray diffraction data were collected at room temperature on an Xcalibur S Oxford Diffraction diffractometer with graphite monochromatized $MoK\alpha$ radiation ($\lambda = 0.71073 \text{ \AA}$) and a CCD detector using the ω scanning mode. The raw data were integrated and then scaled, merged, and corrected for Lorentz-polarization effects using the CrysAlis package [41]. The $C2/c$ (No. 15) space group was chosen based on the reflection statistics and confirmed by the successful refinement of the crystal structure. The experimental details of the data collection and refinement are listed in Table 1.

The structural determinations and refinements were carried out using the Jana2006 program package [42]. Atomic scattering factors for neutral atoms together with anomalous dispersion corrections were taken from International Tables for Crystallography [43]. Illustrations were produced with the Jana2006 program package in combination with the program DIAMOND 3 [44]. The distribution of cations on the structural A -, $M1$, and $M2$ -sites was proposed taking into account site-scattering factors [45], interatomic distances and ionic radii of the cations. Table 2 lists the fractional atomic coordinates, occupancies, site symmetries and equivalent atomic displacement parameters (U_{eq}). Selected interatomic distances are given in Table 3. CDS 2042360 contains the supplementary crystallographic data for this paper. These data can be obtained free of charge via

www.ccdc.cam.ac.uk/data_request/cif, accessed on 24 February 2021, or by emailing data_request@ccdc.cam.ac.uk, or by contacting The Cambridge Crystallographic Data Centre, 12, Union Road, Cambridge CB2 1EZ, UK, fax: +44 1223 336033.

Table 1. Crystal data, data collection and refinement procedural results.

Crystal Data	
Formula	NaMnNi ₂ (H ₂ / ₃ PO ₄) ₃
Formula weight (g)	482.2
Temperature (K)	293(2)
Cell setting	Monoclinic
Space group	C2/c (N ^o 15)
Lattice parameters	
<i>a</i> (Å)	12.019(3)
<i>b</i> (Å); β (°)	12.1217(18), 114.30(3)
<i>c</i> (Å)	6.5549(16)
<i>V</i> (Å ³)	870.4(4)
<i>Z</i>	4
Calculated density, <i>D_x</i> (g cm ⁻³)	3.680
Crystal size (mm)	0.04 × 0.05 × 0.11
Crystal form	Irregular grain
Crystal color	Yellow
Data Collection	
Diffractometer	Xcalibur Oxford Diffraction (CCD-detector)
Radiation, λ	MoK α , 0.7107
Absorption coefficient, μ (mm ⁻¹)	6.387
<i>F</i> (000)	932
Data range θ (°), <i>h</i> , <i>k</i> , <i>l</i>	4.48–34.91, −19 < <i>h</i> < 17, −19 < <i>k</i> < 15, −8 < <i>l</i> < 10
No. of measured reflections	4723
Total reflections (<i>N</i> _{tot})/unique (<i>N</i> _{ref})	708/535
<i>R</i> _{int} (%)	11.12
Criterion for observed reflections	<i>I</i> > 2 σ (<i>I</i>)
Refinement	
Refinement on	Full-matrix least squares on <i>F</i> ²
Weight scheme	1/(σ^2I + 0.0001I)
<i>R</i> ₁ / <i>wR</i> ₂	4.93/9.48
GOF (Goodness of fit)	1.01
Min./max. residual e density, (eÅ ⁻³)	−0.78/0.76

Table 2. Fractional site coordinates, equivalent displacement parameters (*U*_{eq}, Å²), site multiplicities (Mult.), the number of electrons associated with the atoms at the site (*e*_{calc}), and site composition for NaMnNi₂(H₂/₃PO₄)₃.

Site	<i>x</i>	<i>y</i>	<i>z</i>	<i>U</i> _{eq}	Mult.	<i>e</i> _{calc}	Composition
A1'	0.5	0.0361(5)	−0.25	0.029(2)	4	10.08	Na
M1	0.5	0.2806(1)	0.25	0.0095(7)	4	24.58	Mn
M2	0.7132(1)	0.1634(1)	0.1294(2)	0.0121(5)	8	27.23	Ni
T1	0	0.1888(2)	0.25	0.0091(11)	4		P
T2	0.7811(2)	0.3919(2)	0.3847(3)	0.0088(8)	8		P
O1	0.6592(4)	0.1706(4)	0.3939(9)	0.010(2)	8		O
O2	0.6437(5)	0.4138(4)	0.3391(9)	0.010(2)	8		O
O3	0.6559(5)	0.0023(4)	0.1005(9)	0.010(2)	8		O
O4	0.8959(5)	0.1133(4)	0.2440(10)	0.014(2)	8		O
O5	0.5400(5)	0.2370(4)	−0.0384(9)	0.010(2)	8		O
O6	0.7834(5)	0.3238(4)	0.1901(8)	0.010(2)	8		O

Table 3. Selected interatomic distances (Å) for NaMnNi₂(H₂/₃PO₄)₃.

Bond		Distance, Å	Bond		Distance, Å
A1'	O3	2.327(5) × 2	M1	O5	2.198(7) × 2
	O3	2.490(7) × 2		O1	2.201(5) × 2
	O5	2.745(7) × 2		O2	2.259(5) × 2
	O6	2.996(7) × 2	Mean	2.219	
Mean		2.640	Δ ^{M1}		1.60
M2	O3	2.053(5)	T1	O4	1.538(6) × 2
	O1	2.088(7)		O5	1.554(6) × 2
	O6	2.092(5)	Mean	1.546	
	O4	2.097(6)	T2	O3	1.521(6)
	O5	2.111(5)		O1	1.529(5)
	O6	2.117(6)		O6	1.529(6)
O2	1.575(7)				
Mean		2.093	Mean	1.539	
Δ ^{M2}		0.97			

Bond-valence sums (BVS, Table 4) can be used for the indirect verification of mixed oxygen/hydroxyl site presence in the structure. BVS calculations were calculated using the bond valence parameters for the Na⁺-O, Mn²⁺-O, Ni²⁺-O, and P⁵⁺-O bonds [46].

Table 4. Bond-valence analysis (v.u. = valence units) for NaMnNi₂(H₂/₃PO₄)₃.

Site	A1'	M1	M2	T1	T2	V _{anion}
O1		0.33 _{×2↓}	0.33		1.27	1.93
O2		0.28 _{×2↓}			1.12	1.40
O3	(0.24 + 0.16) _{×2↓}		0.36		1.30	2.06
O4			0.32	1.24 _{×2↓}		1.56
O5	0.08 _{×2↓}	0.33 _{×2↓}	0.31	1.19 _{×2↓}		1.91
O6	0.04 _{×2↓}		0.32 + 0.30		1.27	1.93
V _{cation}	1.04	1.88	1.94	4.86	4.96	

2.3. Topological Analysis and Complexity Calculations

Topological analysis of the frameworks was performed by means of natural tilings (the smallest polyhedral cationic clusters forming a framework) analysis of the 3D cation nets [47]. The complexity parameters were calculated as the Shannon information amounts per atom (I_G) and per reduced unit cell ($I_{G,\text{total}}$) [48,49]. The topological and complexity analysis was done using the ToposPro software [50].

3. Results

3.1. Crystal Structure

The crystal structure of NaMnNi₂(H₂/₃PO₄)₃ (Figure 1) is similar to other members of the alluaudite supergroup [16,17] and is based upon zig-zag chains of edge-sharing M1O₆ and M2O₆ octahedra formed by Mn and Ni atoms, respectively. The mean <M-O> distances in the octahedra (<M1-O> = 2.219 Å; <M2-O> = 2.093 Å) are in good agreement with the ionic radii of these elements ($r(\text{Mn}^{2+}) = 0.83$ Å, $r(\text{Ni}^{2+}) = 0.69$ Å [51]). The chains are linked by P1O₄- and P2O₄-tetrahedra (O = O²⁻, OH⁻) forming a hetero-polyhedral framework that contains two types of channels with hexagonal cross-sections. Sodium atoms fill channel I at the A1'-site with the coordinates ($0 \sim \frac{1}{2} \sim \frac{1}{4}$) at the center of a large eight-vertex polyhedron with the mean distance <A1'-O> = 2.640 Å. The refined detailed crystal chemical formula can be written as (Z = 4): □NaMnNi₂(HPO₄)(H_{0.5}PO₄)₂ (where '□' means vacancy at A2-site).

The systematic of the alluaudite-type compounds has previously been reported on the basis of the distribution of extra-framework cations within the channels [19]. The

studied compounds belongs to the “ $\text{KCd}_4(\text{VO}_4)_3$ ” subgroup [52] with the general formula $A2A1'\{M1M2_2(\text{TO}_4)\}$ [19]. The main characteristic feature of **1** is the absence of any cations or H_2O molecules in the channel II [$A(2) = \square$] with the negative charge of the framework balanced by the partial protonation of PO_4 tetrahedra (Table 3). The compound $\text{Na}_2\text{FeNi}_2(\text{PO}_4)_3$ reported in Reference [29] belongs to the same family, but differs from **1** by the presence of Na in both types of channels ($\langle \text{Na}^{(A1')} - \text{O} \rangle = 2.625 \text{ \AA}$, $\langle \text{Na}^{(A2)} - \text{O} \rangle = 2.525 \text{ \AA}$) and by the absence of hydroxyl groups. The M1O_6 - and M2O_6 -octahedra of the heteropolyhedral framework in the compound $\text{Na}_2\text{FeNi}_2(\text{PO}_4)_3$ are occupied by Fe^{3+} and Ni atoms, respectively, with the following mean $\langle M-\text{O} \rangle$ distances: $\langle \text{M1}-\text{O} \rangle = 2.137 \text{ \AA}$, $\langle \text{M2}-\text{O} \rangle = 2.043 \text{ \AA}$ [29].

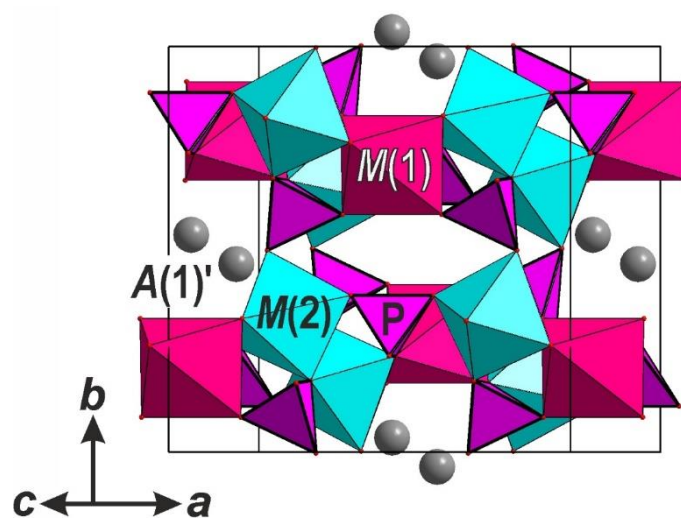


Figure 1. General view of the crystal structure of **1**.

3.2. Hydrogen Bonding

In the crystal structure of **1**, channel II is filled only by statistically disordered hydrogen atoms of P1O_4^- - and P2O_4^- -tetrahedra (Figure 2a). The strong hydrogen bonds are formed between O2-oxygens and O4-oxygens with the distance $\text{O2} \cdots \text{O4} = 2.482(7) \text{ \AA}$ and possible local distributions of hydrogens are shown in Figure 2b–e. Based on the Libowitzky equations [53]:

$$\nu(\text{cm}^{-1}) = 3592 - 304 \times 10^9 \times \exp[-d(\text{O} \cdots \text{O})/0.1321] \quad (1)$$

and

$$\nu(\text{cm}^{-1}) = 3632 - 1.79 \times 10^6 \times \exp[-d(\text{H} \cdots \text{O})/0.2146] \quad (2)$$

the following vibrations should be observed in the IR spectrum: $\sim 1488 \text{ cm}^{-1}$ ($\text{O} \cdots \text{O}$), $\sim 2385 \text{ cm}^{-1}$ ($\text{H} \cdots \text{O}$), and $\sim 2.129 \text{ cm}^{-1}$ ($\text{H} \cdots \text{O}$).

The mixed phosphates-hydrous phosphates are well-known [54–58]. In the crystal structures of $\text{NaMn}_3(\text{PO}_4)(\text{HPO}_4)_2$ [54] and $\text{NaMg}_3(\text{PO}_4)(\text{HPO}_4)_2$ [58] with the localized position of hydrogens the similar scheme of hydrogen bonds is reported. Moreover, for mixed arsenate-hydrous arsenate, a good agreement between observed and calculated stretching vibrations in the IR spectrum was shown [59].

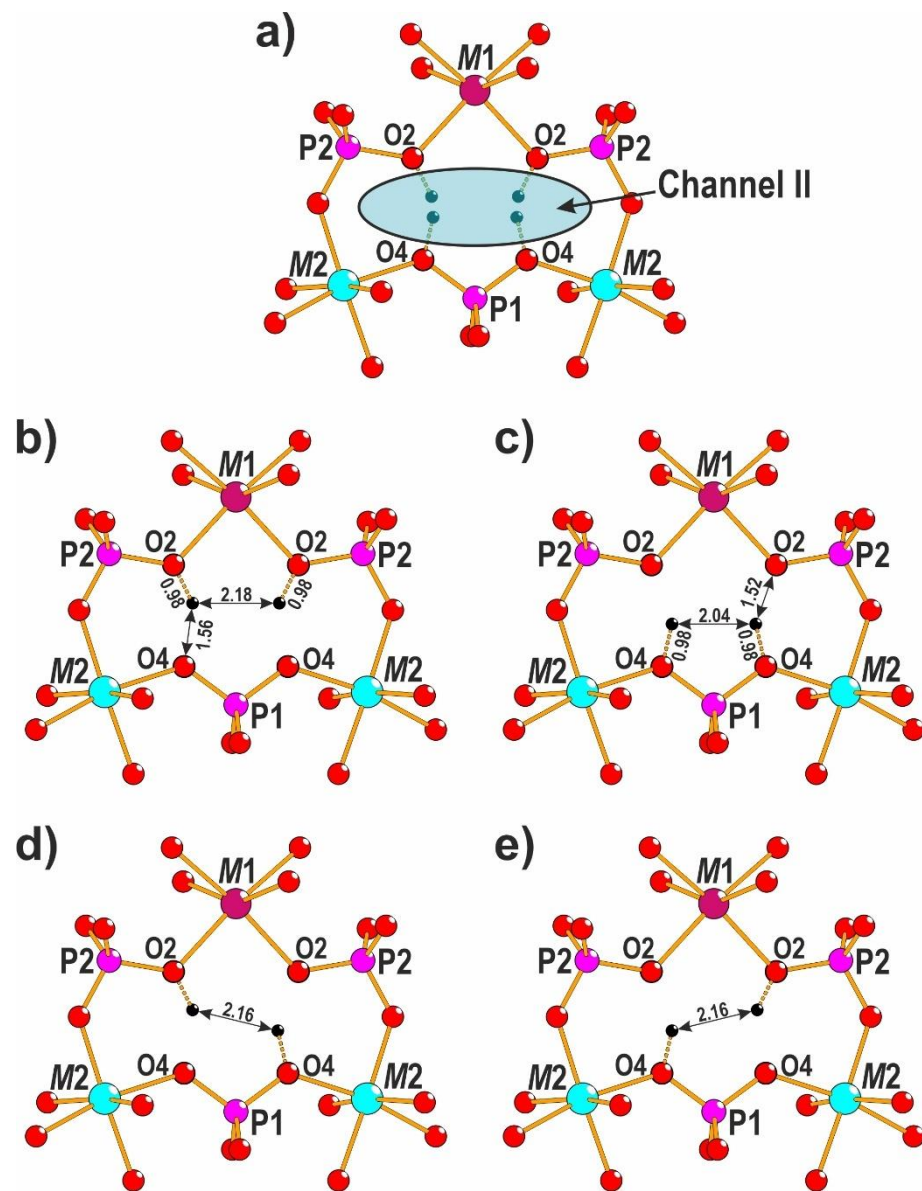


Figure 2. The statistical arrangement of hydrogen atoms in the crystal structure of **1** (a) and possible models of local hydrogen bonds (b–e).

4. Discussion

4.1. General Formula and Stoichiometry of the Alluaudite-type Heteropolyhedral Framework

The crystal structures of minerals and synthetic compounds with the alluaudite structure type are based upon a mixed hetero-polyhedral *MT*-framework of MX_6 -octahedra and TX_4 -tetrahedra [60–62] containing two types of symmetrically non-equivalent $M1X_6$ -octahedra and $M2X_6$ -octahedra and two types of symmetrically non-equivalent $T1X_4$ -tetrahedra and $T2X_4$ -tetrahedra. The anionic *X*-ligands of the framework are represented by bridging O atoms shared between two (p^{II} -ligands [60,61]) as well as three *M* and *T* cations (p^{III} -ligands). The general crystal chemical formula of the framework (taking into account the degree of sharing of *X*-ligands) can be written as:

$$\left\{ M1(M2)_2 \left(T1X_{2(p^{II}+p^{III})} \right) \left(T2X_{2(p^{II}+p^{III})} \right)_2 \right\}^W \quad (3)$$

or

$$\left\{ M1(M2)_2 T1(T2)_2 X_{6(p^{II}+p^{III})} \right\}^W, \quad (4)$$

which the charge (**W**) determined by the oxidation states of the *M*-cations and *T*-cations.

As it was mentioned above, in the majority of the alluaudite-type structures, the anionic *X*-ligands are represented by the oxygen atoms. However, in the case of the charge deficiency of bridging p^{II} -ligands, they could be partially protonated and Equation (4) can be rewritten as:

$$\left\{ M1(M2)_2T1(T2)_2X_{6((1-x)p^{\text{II}}+p^{\text{III}})}X'_{6xp^{\text{II}}} \right\}^{\text{W}}. \quad (5)$$

If $X = \text{O}^{2-}$ and $X' = (\text{OH})^-$, Formula (5) can also be modified as:

$$\left\{ M1(M2)_2T1(T2)_2\text{O}_{6((1-x)p^{\text{II}}+p^{\text{III}})}\text{OH}_{6xp^{\text{II}}} \right\}^{\text{W}}, \quad (6)$$

where $x = 0-1$. The charge of the alluaudite-type framework can be defined using the following equation:

$$\mathbf{W} = V_{M1} + 2V_{M2} + V_{T1} + 2V_{T2} - 24 + 6x, \quad (7)$$

where V_M and V_T are the valences of the *M* and *T* cations, respectively.

The simplified formula is:

$$\left\{ M_3(\text{TO}_{4-2x}\text{OH}_{2x})_3 \right\}^{\text{W}}. \quad (8)$$

Formulas (5) and (6) indicate that the electroneutral framework ($\mathbf{W} = 0$) is possible in the case of $M = \text{Me}^{2+}$ (e.g., $\text{Me} = \text{Mn}^{2+}$, Ni^{2+} , etc.), $T = \text{T}^{6+}$ (S^{6+} , Se^{6+} , Mo^{6+} , etc.), and $x = 0$. However, such alluaudite-type compounds with the neutral frameworks have not been found so far and, typically, the framework has a negative charge ($\mathbf{W} < 0$) balanced by the extra-framework *A*-type cations. Large *A*-cations as well as H_2O molecules may occupy channels of two types characterized by the different topologies: $[3^2.4^2.6^{2/2}]$ (channel I) and $[3^8.4^4.6^{2/2}]$ (channel II) (Figure 3). The alluaudite-type framework density [8] is $27.57 (M+T)/1000 \text{ \AA}$ and the information-based complexity parameters [48,49] are: $v = 36$ atoms, $I_G = 3.281 \text{ bit/atom}$, and $I_{G,\text{total}} = 118.117 \text{ bit/unit cell}$.

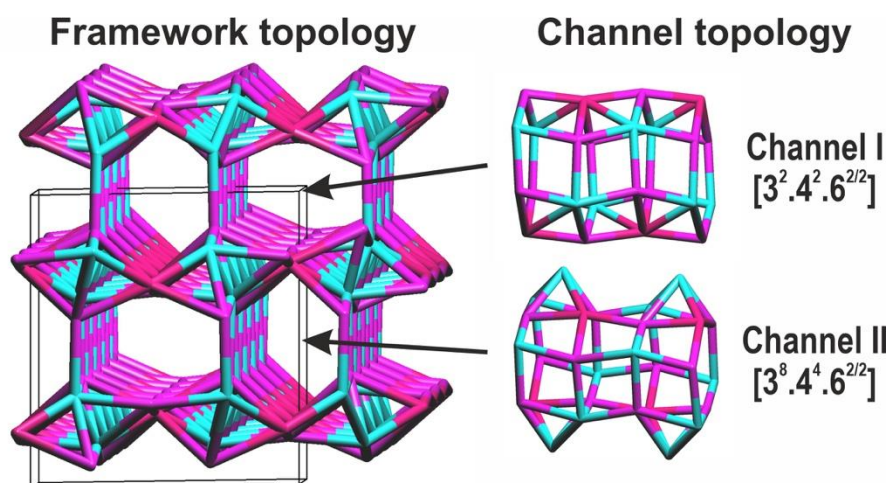


Figure 3. General view of the topology of the alluaudite-type framework and channels I and II.

In accordance with the rules for the description of ordered microporous and mesoporous materials with inorganic hosts approved by the International Zeolite Association, the crystal chemical formula for such a material has to be written in the following order: $\{ \text{guest composition} \} [\text{host composition}]_h \{ \text{dimensionality of the host } D^h \}_p \{ \text{dimensionality of the pore system } D^p \text{--shape of the pore } n_i^{m_i} \text{--direction of the channel } [uvw] \}$ (symmetry) [44,45].

Consequently, the general crystal chemical formula of the studied compounds and related materials (Table 3) can be written as follows ($Z = 1$):

$$\left\{ A_{2-y}^{[4-8]}(\square, \text{H}_2\text{O})_y \left[M_3^{[6]} \left(T^{[4]} \text{O}_{4-2x} \text{OH}_{2x} \right)_3 \right]_h \{3\}_p \left\{ \begin{array}{l} 1 \left[3^2 4^2 6^{2/2} \right] [001] \\ 1 \left[3^8 4^4 6^{2/2} \right] [001] \end{array} \right\} \right\} (C2/c), \quad (9)$$

That indicates that (1) the guests are A -cations (with the coordination numbers ranging from 4 to 8) and H_2O molecules, and (2) the 3D host structure is formed by octahedral M -cations and tetrahedral T -cations and consists of two different, unidimensional channels extending along $[001]$ with the topologies $[3^2 4^2 6^{2/2}]$ and $[3^8 4^4 6^{2/2}]$ [both channels have a 6-membered ring (6R) pore opening], respectively.

4.2. The Influence of the Hetero-Polyhedral Substitutions at Extraframework A -Sites on the Stoichiometry of the Alluaudite-Type Framework

In the alluaudite-type structures, extra-framework alkaline and alkaline-earth A -cations may possess high mobility and migrate along the channels. Moreover, transition metal cations can also fill the channels through incorporation into the $A(1)'$ -site (the $4e$ Wyckoff site with the coordinates $(0 \ y \ \frac{1}{4})$, $y \sim 0.25$) or $A(2)$ -site (the $4a$ site with the coordinates $(0 \ 0 \ 0)$) in the centers of flat squares. The incorporation of these elements changes the ratio between the p^{II} - and p^{III} -type X -ligands as well as the topology of the framework. As a result, Formula (4) can be rewritten as:

$$\left\{ A(1)' M1(M2)_2 T1(T2)_2 X_{2p^{\text{II}}+10p^{\text{III}}} \right\}^{\text{W}} \quad (10)$$

or

$$\left\{ A(2) M1(M2)_2 T1(T2)_2 X_{2p^{\text{II}}+10p^{\text{III}}} \right\}^{\text{W}}, \quad (11)$$

where $x = 0-1$. The derivative of the alluaudite-type framework containing occupied $A(1)'$ sites is described by the formula (10) and can be denoted as the johillerite-type (by the analogy with the mineral johillerite, $\text{NaCuMgMg}_2(\text{AsO}_4)_3$ [63,64]), while the derivative with the occupied $A(2)$ sites and the formula (11) is denoted as the $\text{KCd}_3(\text{VO}_4)_3$ -type [52,65]. Taking into account that both derivatives also contain bridging p^{II} -type X -ligands that can be partially protonated, Formulas (10) and (11) can be modified as:

$$\left\{ A(1)' M1(M2)_2 T1(T2)_2 X_{2((1-x)p^{\text{II}}+5p^{\text{III}})} X'_{2xp^{\text{II}}} \right\}^{\text{W}} \quad (12)$$

or

$$\left\{ A(2) M1(M2)_2 T1(T2)_2 X_{2((1-x)p^{\text{II}}+5p^{\text{III}})} X'_{2xp^{\text{II}}} \right\}^{\text{W}}. \quad (13)$$

If $X = \text{O}^{2-}$ and $X' = \text{OH}^-$, Formulas (12) and (13) can be simplified by the following.

$$\left\{ AM_3(\text{TO}_{4-0.66x}\text{OH}_{0.66x})_3 \right\}^{\text{W}}. \quad (14)$$

The keyite-type derivative of the alluaudite-type framework is characterized by the presence of transition metals in both $A(1)'$ and $A(2)$ sites. Its general formula can be written as:

$$\left\{ A(1)' A(2) M1(M2)_2 T1(T2)_2 X_{12p^{\text{III}}} \right\}^{\text{W}} \quad (15)$$

Because of the absence of the p^{II} -type X -ligands, the protonation is no longer possible ($X = \text{O}^{2-}$) and the simplified formula of the keyite-type derivative (named after the mineral keyite, $(\square_{0.5}\text{Cu}_{0.5})\text{CuCdZn}_2(\text{AsO}_4)_3 \cdot \text{H}_2\text{O}$ [66]) is:

$$\left\{ A_2 M_3(\text{TO}_4)_3 \right\}^{\text{W}} \quad (16)$$

4.3. Topological Features of Alluaudite-Type Framework and Its Derivatives

The presence of transition metals at the *A* sites of the alluaudite-type framework results in the changes of stoichiometry and the local topological features. The topological analysis using a ToposPro software [50] makes it possible to find common tilings in generally similar heteropolyhedral frameworks of alluaudite-type and its derivatives (the johillerite, $\text{KCd}_4(\text{VO}_4)_3$, and keyite types) and to investigate their differences.

An ‘empty’ parent alluaudite-type framework consists of four natural tilings: $(2T3M)$ -[43] (formed by two *T*-cations and three *M*-cations), $(2T3M)$ -[3².4²], $(4T5M)$ -[3².4².6²], and $(6T8M)$ -[3⁸.4⁴.6²] (Figure 4a). The occupancy of the *A* sites by additional transition metal cations changes the topology of its derivatives significantly. The johillerite-type derivative (with the occupied *A*(1)[′]-site in channel **I**) is formed by five types of natural tiles. Among them, the $(2T3M)$ -[43], $(2T3M)$ -[3².4²], and $(4T5M)$ -[3².4².6²] tilings are identical to those in the parent alluaudite-type framework, while the $(6T8M2A)$ -[3²⁰.4⁴] and $(2T4M)$ -[3⁴.4²] tilings are unique (Figure 4b). The $\text{KCd}_4(\text{VO}_4)_3$ -type derivative (the *A*(2)-site is occupied in channel **II**) is also characterized by the presence of five types of tilings: the $(2T3M)$ -[3².4²] and $(4T5M)$ -[3².4².6²] tilings are identical to those of the parent framework, while the $(3T5M2A)$ -[3¹⁰.4³], $(3T2M1A)$ -[3².4³], and $(2T4M)$ -[3⁴.4²] tilings are unique (Figure 4c). In the keyite-type derivative (both channels **I** and **II** are filled by cations at the *A*(1)[′]- and *A*(2)-sites). There are five types of natural tilings (Figure 4d): $(2T3M)$ -[43] is identical to that in the parent structure, while the $(6T8M2A)$ -[3²⁰.4⁴] tiling is identical to that in johillerite. The $(1T2M1A)$ -[34], $(2T3M1A)$ -[3⁴.4²] (topologically identical to other [3⁴.4²] tilings, but chemically different) and $(3T3M2A)$ -[3⁶.4³] tilings are unique and appear due to the presence of cations in both types of channels. Comparative data on the general features of the alluaudite-type frameworks and its derivatives are summarized in Table 5.

Table 5. Crystal data, data collection and refinement procedural results.

Type of the Framework	Natural Tilings	Complexity Parameters		
		<i>v</i> (atoms)	<i>I</i> _G (bit/atom)	<i>I</i> _{G,total} (bit/unit cell)
Alluaudite	[4 ³] ₂ [3 ² .4 ²] ₄ [3 ² .4 ² .6 ²] ₂ [3 ⁸ .4 ⁴ .6 ²]	36	3.281	118.117
Johillerite	[4 ₃] ² [3 ² .4 ²] ₂ [3 ⁴ .4 ²][3 ² .4 ² .6 ²] ₂ [3 ²⁰ .4 ⁴]	38	3.406	129.421
$\text{KCd}_4(\text{VO}_4)_3$	[3 ² .4 ²] ₂ [3 ² .4 ₃] ₂ [3 ⁴ .4 ²][3 ² .4 ² .6 ²] ₂ [3 ¹⁰ .4 ³] ₂	38	3.406	129.421
Keyite	[4 ³] ₂ [3 ⁴] ₂ [3 ⁴ .4 ²] ₃ [3 ⁶ .4 ³] ₂ [3 ²⁰ .4 ⁴]	40	3.522	140.877

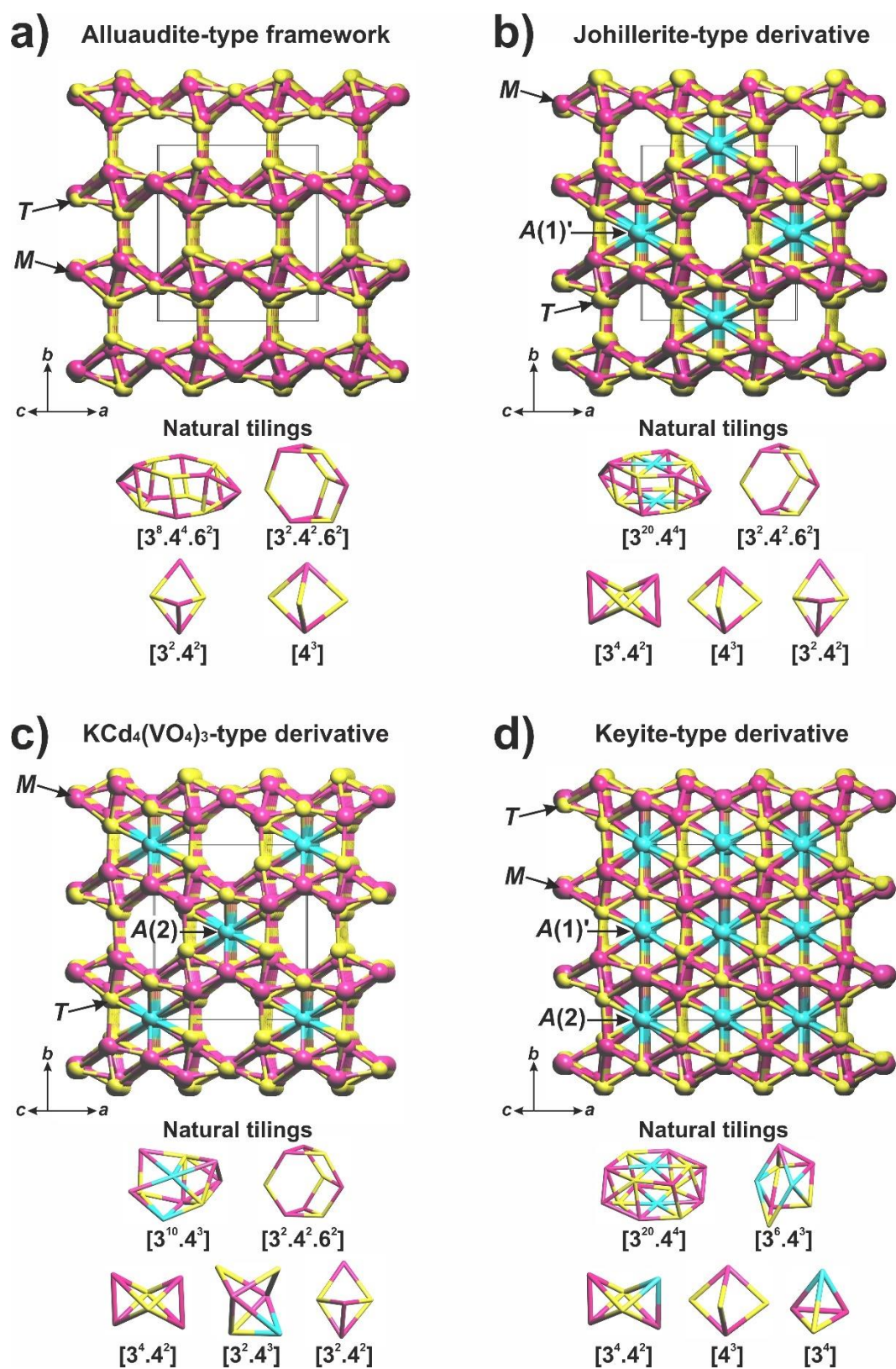


Figure 4. Alluaudite type framework (a) and its derivatives: johillerite-type (b), $\text{KCd}_4(\text{VO}_4)_3$ -type (c), and keyite-type (d). General view and natural tilings.

5. Conclusions

The occupancy of the *A* sites by additional transition metal cations significantly changes the topology of its derivatives. Detailed analysis of the alluaudite-type framework as well as its derivatives shows the influence of the different types of the cation arrangement within extra-framework sites on the stoichiometry (the possible amount of OH groups), complexity parameters of the frameworks, and types of natural tiling.

Author Contributions: Conceptualization, S.M.A., N.A.Y. and S.V.K. Synthesis, A.S.V. and O.V.D. Formal analysis, N.A.K., O.A.G., and D.V.D. Writing—original draft preparation, S.M.A., N.A.Y., and S.V.K. Supervision, S.V.K. All authors have read and agreed to the published version of the manuscript.

Funding: This research was funded by the Russian Science Foundation, grant numbers 20-77-10065 (Topological and modular analysis; complexity calculations) and 19-77-10013 (Single-crystal X-ray analysis).

Acknowledgments: The authors are grateful to three reviewers and the Special issue editors Igor V. Pekov and Natalia V. Zubkova for their useful comments and suggestions.

Conflicts of Interest: The authors declare no conflict of interest.

References

1. Sanz, F.; Parada, C.; Rojo, J.M.; Ruíz-Valero, C. Synthesis, structural characterization, magnetic properties, and ionic conductivity of $\text{Na}_4\text{MII}_3(\text{PO}_4)_2(\text{P}_2\text{O}_7)$ (M II = Mn, Co, Ni). *Chem. Mater.* **2001**, *13*, 1334–1340. [[CrossRef](#)]
2. De Pedro, I.; Rojo, J.M.; Jubera, V.; Fernández, J.R.; Marcos, J.S.; Lezama, L.; Rojo, T. Effect of Ni_2^+ ($S = 1$) and Cu_2^+ ($S = \frac{1}{2}$) substitution on the antiferromagnetic ordered phase $\text{Co}_2(\text{OH})_4$ with spin glass behaviour. *J. Mater. Chem.* **2004**, *14*, 1157–1163. [[CrossRef](#)]
3. Yamnova, N.A.; Aksenov, S.M.; Mironov, V.S.; Volkov, A.S.; Borovikova, E.Y.; Gurbanova, O.A.; Dimitrova, O.V.; Deyneko, D.V. The first layer potassium–bismuth–nickel oxophosphate $\text{KBi}_4\text{Ni}_2(\text{PO}_4)_3\text{O}_4$: Synthesis, crystal structure, and expected magnetic properties. *Crystallogr. Rep.* **2017**, *62*. [[CrossRef](#)]
4. Aksenov, S.M.; Mironov, V.S.; Borovikova, E.Y.; Yamnova, N.A.; Gurbanova, O.A.; Volkov, A.S.; Dimitrova, O.V.; Deyneko, D.V. Synthesis, crystal structure, vibrational spectroscopy and expected magnetic properties of a new bismuth nickel phosphate $\text{Ni}(\text{BiO})_2(\text{PO}_4)(\text{OH})$ with a namibite-type structure. *Solid State Sci.* **2017**, *63*. [[CrossRef](#)]
5. Li, X.; Xiao, X.; Li, Q.; Wei, J.; Xue, H.; Pang, H. Metal (M = Co, Ni) phosphate based materials for high-performance supercapacitors. *Inorg. Chem. Front.* **2018**, *5*, 11–28. [[CrossRef](#)]
6. Rommel, S.M.; Schall, N.; Brünig, C.; Wehrich, R. Challenges in the synthesis of high voltage electrode materials for lithium-ion batteries: A review on LiNiPO_4 . *Mon. Chem. Chem. Mon.* **2014**, *145*, 385–404. [[CrossRef](#)]
7. Herle, P.S.; Ellis, B.; Coombs, N.; Nazar, L.F. Nano-network electronic conduction in iron and nickel olivine phosphates. *Nat. Mater.* **2004**, *3*, 147–152. [[CrossRef](#)] [[PubMed](#)]
8. Chukanov, N.V.; Pekov, I.V.; Rastsvetaeva, R.K. Crystal chemistry, properties and synthesis of microporous silicates containing transition elements. *Russ. Chem. Rev.* **2004**, *73*, 205–223. [[CrossRef](#)]
9. Rocha, J.; Lin, Z. Microporous Mixed Octahedral-Pentahedral-Tetrahedral Framework Silicates. *Rev. Mineral. Geochem.* **2005**, *57*, 173–201. [[CrossRef](#)]
10. Rocha, J.; Anderson, M.W. Microporous titanosilicates and other novel mixed octahedral-tetrahedral framework oxides. *Eur. J. Inorg. Chem.* **2000**, *2000*, 801–818. [[CrossRef](#)]
11. Li, Y.; Yu, J. New stories of zeolite structures: Their descriptions, determinations, predictions, and evaluations. *Chem. Rev.* **2014**, *114*, 7268–7316. [[CrossRef](#)]
12. Guillou, N.; Gao, Q.; Nogues, M.; Morris, R.E.; Hervieu, M.; Férey, G.; Cheetham, A.K. Zeolitic and magnetic properties of a 24-membered ring porous nickel(II) phosphate, VSB-1. *Comptes Rendus l'Académie Sci. Ser. IIC Chem.* **1999**, *2*, 387–392. [[CrossRef](#)]
13. Garcia, R.; Philp, E.F.; Slawin, A.M.Z.; Wright, P.A.; Cox, P.A. Nickel complexed within an azamacrocyclic structure directing agent in the crystallization of the framework metalloaluminophosphates STA-6 and STA-7. *J. Mater. Chem.* **2001**, *11*, 1421–1427. [[CrossRef](#)]
14. Guillou, N.; Gao, Q.; Forster, P.M.; Chang, J.-S.; Noguès, M.; Park, S.-E.; Férey, G.; Cheetham, A.K. Nickel(II) Phosphate VSB-5: A magnetic nanoporous hydrogenation catalyst with 24-ring tunnels. *Angew. Chemie Int. Ed.* **2001**, *40*, 2831–2834. [[CrossRef](#)]
15. Dechambenoit, P.; Long, J.R. Microporous magnets. *Chem. Soc. Rev.* **2011**, *40*, 3249. [[CrossRef](#)]
16. Moore, P.B. Crystal chemistry of the alluaudite structure type: Contribution to the paragenesis of pegmatite phosphate giant crystals. *Am. Mineral.* **1971**, *56*, 1955–1975.
17. Hatert, F. A new nomenclature scheme for the alluaudite supergroup. *Eur. J. Mineral.* **2019**, *31*, 807–822. [[CrossRef](#)]
18. Đorđević, T.; Wittwer, A.; Krivovichev, S.V. Three new alluaudite-like protonated arsenates: $\text{NaMg}_3(\text{AsO}_4)(\text{AsO}_3\text{OH})_2$, $\text{NaN}_3(\text{AsO}_4)(\text{AsO}_3\text{OH})_2$ and $\text{Na}(\text{Na}_{0.6}\text{Zn}_{0.4})\text{Zn}_2(\text{H}_{0.6}\text{AsO}_4)(\text{AsO}_3\text{OH})_2$. *Eur. J. Mineral.* **2015**, *27*, 559–573. [[CrossRef](#)]

19. Yakubovich, O.V.; Kiryukhina, G.V.; Dimitrova, O.V. Crystal chemistry of $\text{KCuMn}_3(\text{VO}_4)_3$ in the context of detailed systematics of the alluaudite family. *Crystallogr. Rep.* **2016**, *61*, 566–575. [[CrossRef](#)]
20. Hatert, F.; Keller, P.; Lissner, F.; Antenucci, D.; Fransolet, A.-M. First experimental evidence of alluaudite-like phosphates with high Li-content: The $(\text{Na}_{1-x}\text{Li}_x)\text{MnFe}_2(\text{PO}_4)_3$ series ($x = 0$ to 1). *Eur. J. Mineral.* **2000**, *12*, 847–857. [[CrossRef](#)]
21. Krivovichev, S.V.; Vergasova, L.P.; Filatov, S.K.; Rybin, D.S.; Britvin, S.N.; Ananiev, V.V. Hatertite, $\text{Na}_2(\text{Ca},\text{Na})(\text{Fe}^{3+},\text{Cu})_2(\text{AsO}_4)_3$, a new alluaudite-group mineral from Tolbachik fumaroles, Kamchatka peninsula, Russia. *Eur. J. Mineral.* **2013**, *25*, 683–691. [[CrossRef](#)]
22. Trad, K.; Carlier, D.; Croguennec, L.; Wattiaux, A.; Ben Amara, M.; Delmas, C. $\text{NaMnFe}_2(\text{PO}_4)_3$ Alluaudite phase: Synthesis, structure, and electrochemical properties as positive electrode in lithium and sodium batteries. *Chem. Mater.* **2010**, *22*, 5554–5562. [[CrossRef](#)]
23. Barpanda, P.; Oyama, G.; Nishimura, S.; Chung, S.-C.; Yamada, A. A 3.8-V earth-abundant sodium battery electrode. *Nat. Commun.* **2014**, *5*, 4358. [[CrossRef](#)]
24. Xu, K. Electrolytes and interphases in Li-Ion batteries and beyond. *Chem. Rev.* **2014**, *114*, 11503–11618. [[CrossRef](#)]
25. Dwibedi, D.; Araujo, R.B.; Chakraborty, S.; Shanbogh, P.P.; Sundaram, N.G.; Ahuja, R.; Barpanda, P. $\text{Na}_{2.44}\text{Mn}_{1.79}(\text{SO}_4)_3$: A new member of the alluaudite family of insertion compounds for sodium ion batteries. *J. Mater. Chem. A* **2015**, *3*, 18564–18571. [[CrossRef](#)]
26. Wong, L.L.; Chen, H.M.; Adams, S. Sodium-ion diffusion mechanisms in the low cost high voltage cathode material $\text{Na}_{2+\delta}\text{Fe}_{2-\delta/2}(\text{SO}_4)_3$. *Phys. Chem. Chem. Phys.* **2015**, *17*, 9186–9193. [[CrossRef](#)]
27. Meng, Y.; Yu, T.; Zhang, S.; Deng, C. Top-down synthesis of muscle-inspired alluaudite $\text{Na}_{2+2x}\text{Fe}_{2-x}(\text{SO}_4)_3/\text{SWNT}$ spindle as a high-rate and high-potential cathode for sodium-ion batteries. *J. Mater. Chem. A* **2016**, *4*, 1624–1631. [[CrossRef](#)]
28. Lu, J.; Nishimura, S.; Yamada, A. Polyanionic solid-solution cathodes for rechargeable batteries. *Chem. Mater.* **2017**, *29*, 3597–3602. [[CrossRef](#)]
29. Essehli, R.; Bali, B.E.; Benmokhtar, S.; Bouziane, K.; Manoun, B.; Abdalislam, M.A.; Ehrenberg, H. Crystal structures and magnetic properties of iron (III)-based phosphates: $\text{Na}_4\text{NiFe}(\text{PO}_4)_3$ and $\text{Na}_2\text{Ni}_2\text{Fe}(\text{PO}_4)_3$. *J. Alloys Compd.* **2011**, *509*, 1163–1171. [[CrossRef](#)]
30. Harbaoui, D.; Sanad, M.M.S.; Rossignol, C.; Hlil, E.K.; Amdouni, N.; Obbade, S. Synthesis and structural, electrical, and magnetic properties of new Iron–Aluminum alluaudite phases $\beta\text{-Na}_2\text{Ni}_2\text{M}(\text{PO}_4)_3$ ($\text{M} = \text{Fe}$ and Al). *Inorg. Chem.* **2017**, *56*, 13051–13061. [[CrossRef](#)]
31. Ouaatta, S.; Assani, A.; Saadi, M.; El Ammari, L. Crystal structure of calcium dinickel(II) iron(III) tris(orthophosphate): $\text{CaNi}_2\text{Fe}(\text{PO}_4)_3$. *Acta Crystallogr. Sect. E Crystallogr. Commun.* **2017**, *73*, 893–895. [[CrossRef](#)]
32. Ben Smail, R.; Jouini, T. $\text{AgNi}_3(\text{PO}_4)(\text{HPO}_4)_2$: An alluaudite-like structure. *Acta Crystallogr. Sect. C Cryst. Struct. Commun.* **2002**, *58*, i61–i62. [[CrossRef](#)]
33. Dwibedi, D.; Barpanda, P. Solution-assisted Energy-savvy Synthesis of High-voltage $\text{Na}_2\text{M}_2(\text{SO}_4)_3$ ($\text{M} = 3d$ metals) alluaudite family of sodium insertion materials. *Mater. Today Proc.* **2018**, *5*, 23439–23442. [[CrossRef](#)]
34. Marinova, D.M.; Kukeva, R.R.; Zhecheva, E.N.; Stoyanova, R.K. Selective sodium intercalation into sodium nickel–manganese sulfate for dual Na–Li-ion batteries. *Phys. Chem. Chem. Phys.* **2018**, *20*, 12755–12766. [[CrossRef](#)]
35. Driscoll, L.L.; Kendrick, E.; Knight, K.S.; Wright, A.J.; Slater, P.R. Investigation into the dehydration of selenate doped $\text{Na}_2\text{M}(\text{SO}_4)_2 \cdot 2\text{H}_2\text{O}$ ($\text{M} = \text{Mn}, \text{Fe}, \text{Co}$ and Ni): Stabilisation of the high Na content alluaudite phases $\text{Na}_3\text{M}_{1.5}(\text{SO}_4)_3 \cdot 1.5x(\text{SeO}_4) \cdot 1.5x\text{H}_2\text{O}$ ($\text{M} = \text{Mn}, \text{Co}$ and Ni) through selenate incorporation. *J. Solid State Chem.* **2018**, *258*, 64–71. [[CrossRef](#)]
36. Aksenov, S.M.; Mackley, S.A.; Deyneko, D.V.; Taroev, V.K.; Tauson, V.L.; Rastsvetaeva, R.K.; Burns, P.C. Crystal chemistry of compounds with lanthanide based microporous heteropolyhedral frameworks: Synthesis, crystal structures, and luminescence properties of novel potassium cerium and erbium silicates. *Microporous Mesoporous Mater.* **2019**, *284*, 25–35. [[CrossRef](#)]
37. Aksenov, S.M.; Chukanov, N.V.; Pekov, I.V.; Rastsvetaeva, R.K.; Hixon, A.E. Crystal structure and topological features of manganonaujakasite, a mineral with microporous heteropolyhedral framework related to AlPO-25 (ATV). *Microporous Mesoporous Mater.* **2019**, *279*, 128–132. [[CrossRef](#)]
38. Dal Bo, F.; Aksenov, S.M.; Burns, P.C. A novel family of microporous uranyl germanates: Framework topology and complexity of the crystal structures. *J. Solid State Chem.* **2019**, *271*, 126–134. [[CrossRef](#)]
39. Chong, S.; Aksenov, S.M.; Dal Bo, F.; Perry, S.N.; Dimakopoulou, F.; Burns, P.C. Framework polymorphism and modular crystal structures of uranyl vanadates of divalent cations: Synthesis and characterization of $\text{M}(\text{UO}_2)(\text{V}_2\text{O}_7)$ ($\text{M} = \text{Ca}, \text{Sr}$) and $\text{Sr}_3(\text{UO}_2)(\text{V}_2\text{O}_7)_2$. *Z. Anorg. Allg. Chem.* **2019**, *645*, 981–987. [[CrossRef](#)]
40. Zhang, L.; Aksenov, S.M.; Kokot, A.M.; Perry, S.N.; Olds, T.A.; Burns, P.C. Crystal chemistry and structural complexity of Uranium(IV) sulfates: Synthesis of $\text{U}_3\text{H}_2(\text{SO}_4)_7(\text{H}_2\text{O})_5 \cdot 3\text{H}_2\text{O}$ and $\text{U}_3(\text{UO}_2)_{0.2}(\text{SO}_4)_6(\text{OH})_{0.4} \cdot 2.3\text{H}_2\text{O}$ with Framework structures by the photochemical reduction of uranyl. *Inorg. Chem.* **2020**, *59*, 5813–5817. [[CrossRef](#)] [[PubMed](#)]
41. Oxford Diffraction. *CrysAlisPro*; Oxford Diffraction Ltd.: Abingdon, UK, 2009.
42. Petricek, V.; Dusek, M.; Palatinus, L. Crystallographic computing system JANA2006: General features. *Z. Krist.* **2014**, *229*, 345–352.
43. Prince, E. (Ed.) *International Tables for Crystallography*; International Union of Crystallography: Chester, UK, 2006; Volume C, ISBN 978-1-4020-1900-5.
44. Brandenburg, K.; Putz, H. *DIAMOND, Version 3*; Crystal Impact GbR: Bonn, Germany, 2005.

45. Hawthorne, F.C.; Ungaretti, L.; Oberti, R. Site populations in minerals; terminology and presentation of results of crystal-structure refinement. *Can. Mineral.* **1995**, *33*, 907–911.
46. Brown, I.D.; Altermatt, D. Bond-valence parameters obtained from a systematic analysis of the Inorganic Crystal Structure Database. *Acta Crystallogr. Sect. B* **1985**, *41*, 244–247. [[CrossRef](#)]
47. Blatov, V.A.; O’Keeffe, M.; Proserpio, D.M. Vertex-, face-, point-, Schläfli-, and Delaney-symbols in nets, polyhedra and tilings: Recommended terminology. *CrystEngComm* **2010**, *12*, 44–48. [[CrossRef](#)]
48. Krivovichev, S.V. Which inorganic structures are the most complex? *Angew. Chem. Int. Ed.* **2014**, *53*, 654–661. [[CrossRef](#)]
49. Krivovichev, S.V. Structural complexity of minerals: Information storage and processing in the mineral world. *Mineral. Mag.* **2013**, *77*, 275–326. [[CrossRef](#)]
50. Blatov, V.A.; Shevchenko, A.P.; Proserpio, D.M. Applied topological analysis of crystal structures with the program package ToposPro. *Cryst. Growth Des.* **2014**, *14*, 3576–3586. [[CrossRef](#)]
51. Shannon, R.D. Revised effective ionic radii and systematic studies of interatomic distances in halides and chalcogenides. *Acta Crystallogr. Sect. A* **1976**, *32*, 751–767. [[CrossRef](#)]
52. Eddahby, L.; Berrada, A.; Boukhari, A.; Holt, E.M. Potassium cadmium orthovanadate and potassium tetracadmium trisorthovanadate. *Eur. J. Inorg. Chem.* **1997**, *34*, 527–551.
53. Libowitzky, E. Korrelation von O*H-Streckfrequenzen und O*H{ctdot};O-Wasserstoffbrückenlängen in Mineralen. *Mon. Chem. Chem. Mon.* **1999**, *130*, 1047. [[CrossRef](#)]
54. Leroux, F.; Mar, A.; Payen, C.; Guyomard, D.; Verbaere, A.; Piffard, Y. Synthesis and Structure of NaMn₃(PO₄)(HPO₄)₂, an unoxidized variant of the alluaudite structure type. *J. Solid State Chem.* **1995**, *115*, 240–246. [[CrossRef](#)]
55. Leroux, F.; Mar, A.; Guyomard, D.; Piffard, Y. Cation substitution in the alluaudite structure type: Synthesis and structure of AgMn₃(PO₄)(HPO₄)₂. *J. Solid State Chem.* **1995**, *117*, 206–212. [[CrossRef](#)]
56. Cooper, M.A.; Hawthorne, F.C.; Ball, N.A.; Ramik, R.A.; Roberts, A.C. Groatite, Na Ca Mn₂⁺²(PO₄) [PO₃(OH)]₂, a new mineral species of the alluaudite group from the tanco pegmatite, bernic lake, manitoba, Canada: Description and crystal structure. *Can. Mineral.* **2009**, *47*, 1225–1235. [[CrossRef](#)]
57. Assani, A.; El Ammari, L.; Zriouil, M.; Saadi, M. Disilver(I) trinickel(II) hydrogenphosphate bis(phosphate), Ag₂Ni₃(HPO₄)(PO₄)₂. *Acta Crystallogr. Sect. E Struct. Rep. Online* **2011**, *67*, i40. [[CrossRef](#)]
58. Ould Saleck, A.; Assani, A.; Saadi, M.; Mercier, C.; Follet, C.; El Ammari, L. Crystal structure of alluaudite-type NaMg₃(HPO₄)₂(PO₄). *Acta Crystallogr. Sect. E Crystallogr. Commun.* **2015**, *71*, 813–815. [[CrossRef](#)]
59. Stojanović, J.; Đorđević, T.; Karanović, L. Structural features of two novel alluaudite-like arsenates Cd_{1.16}Zn_{2.34}(AsO₄)_{1.5}(HAsO₄)(H₂AsO₄)_{0.5} and Cd_{0.74}Mg_{2.76}(AsO₄)_{1.5}(HAsO₄)(H₂AsO₄)_{0.5}. *J. Alloys Compd.* **2012**, *520*, 180–189. [[CrossRef](#)] [[PubMed](#)]
60. Voronkov, A.A.; Ilyukhin, V.V.; Belov, N.V. Crystal chemistry of mixed frameworks—Principles of their formation. *Kristallografiya* **1975**, *20*, 556–566.
61. Sandomirskiy, P.A.; Belov, N.V. *Crystal Chemistry of Mixed Anionic Radicals*; Nauka: Moscow, Russia, 1984.
62. Ilyushin, G.D.; Blatov, V.A. Crystal chemistry of zirconosilicates and their analogs: Topological classification of MT frameworks and suprapolyhedral invariants. *Acta Crystallogr. Sect. B Struct. Sci.* **2002**, *58*, 198–218. [[CrossRef](#)] [[PubMed](#)]
63. Keller, P.; Hess, H.; Dunn, P.J. Johillerit, Na(Mg,Zn)₃Cu(AsO₄)₃ ein neues mineral aus tsumeb, namibia. *Tschermaks Mineral. Petrogr. Mitt.* **1982**, *29*, 169–175. [[CrossRef](#)]
64. Koshlyakova, N.N.; Zubkova, N.V.; Pekov, I.V.; Giester, G.; Sidorov, E.G. Crystal chemistry of johillerite. *Can. Mineral.* **2018**, *56*, 189–201. [[CrossRef](#)]
65. Holt, E.; Drai, S.; Olazcuaga, R.; Vlasse, M. The crystal structure of cadmium potassium orthovanadate KCd₄(VO₄)₃. *Acta Crystallogr. Sect. B Struct. Crystallogr. Cryst. Chem.* **1977**, *33*, 95–98. [[CrossRef](#)]
66. Malcherek, T.; Schlüter, J. The keyite crystal structure, revisited. *Z. Krist. Cryst. Mater.* **2013**, *228*. [[CrossRef](#)]